Supplementary Information

Tunable Sub-Terahertz Resonant Absorption in High-Coercivity Magnetodielectric Ceramics

Evgeny A. Gorbachev, Liudmila N. Alyabyeva, Artem V. Pronin, Alexandra S. Sultanovskaya, Ekaterina S. Kozlyakova, Oxana V. Magdysyuk, Ilya V. Roslyakov, Martin Dressel, Boris P. Gorshunov, and Lev A. Trusov

§1. Synchrotron XRD, SEM imaging, and magnetic properties
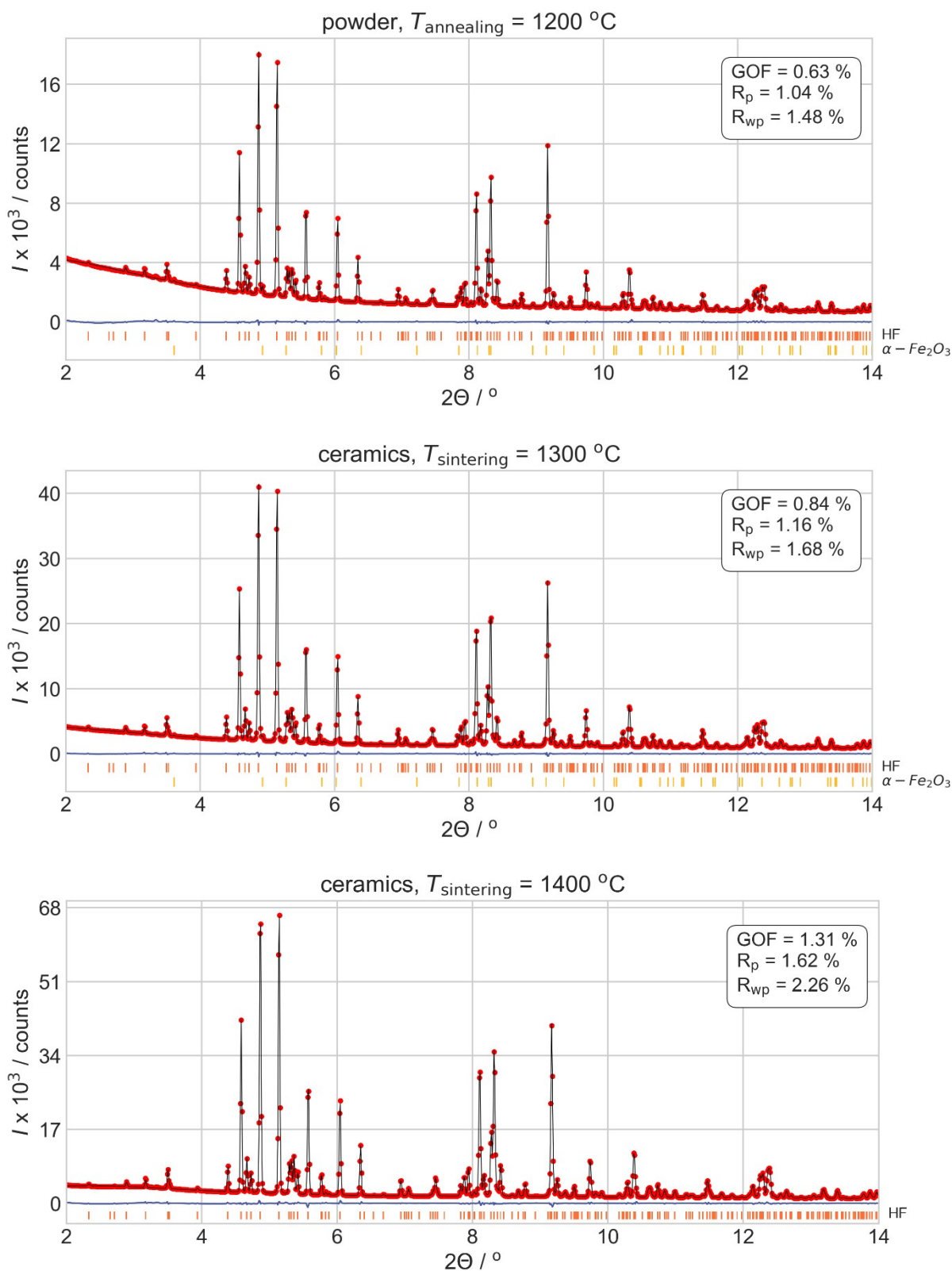

Fig. S1. Rietveld refinement of the hexaferrites: the initial powder (obtained at 1200 °C) and ceramics $Sr_{1-x/12}Ca_{x/12}Fe_{12-x}Al_xO_{19}$ (x = 4) annealed at 1300 and 1400 °C for half an hour. The experimental (red circles) and calculated (black line) data, their difference (blue curve), and the bars correspond to the M-type hexaferrite and α-Fe_2O_3 phases.
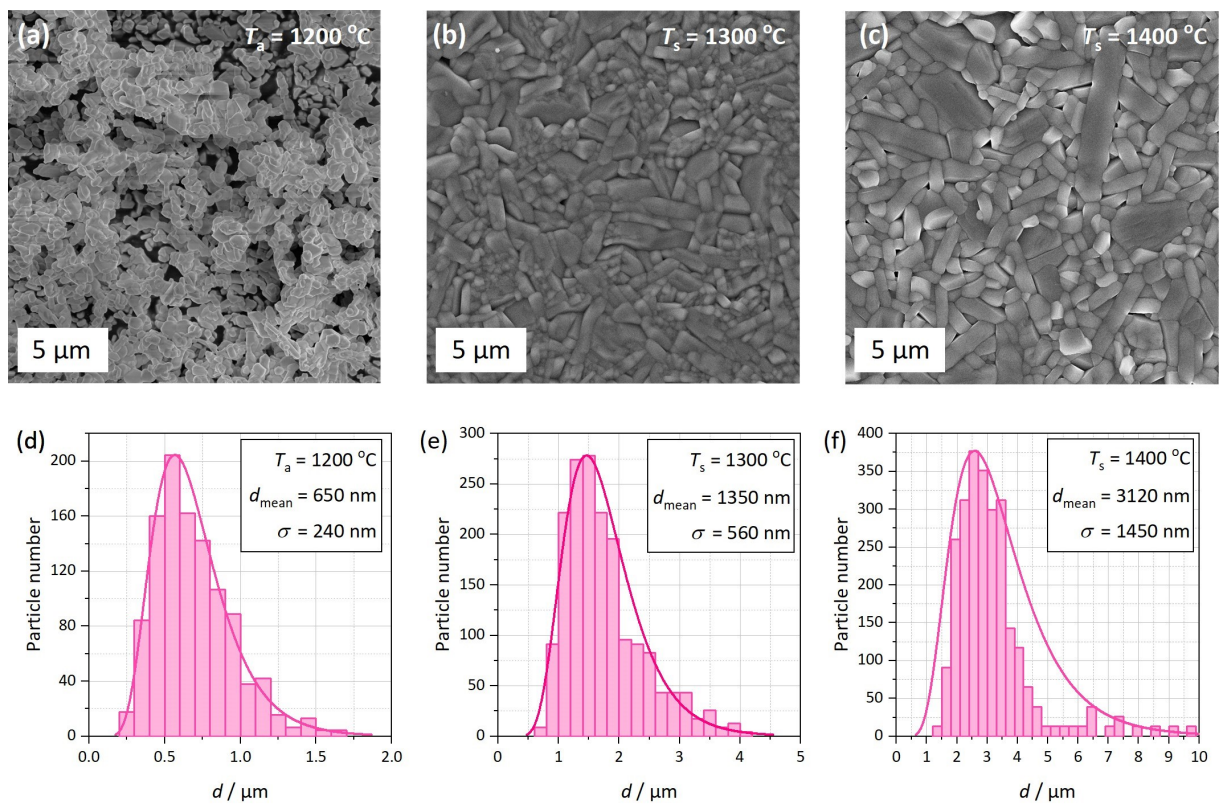
Fig. S2. SEM images (a – c) and particle size distribution histograms (d – e) of the initial hexaferrite powder $Sr_{1-x/12}Ca_{x/12}Fe_{12-x}Al_xO_{19}$ ($x = 4$) and the corresponding ceramics.

Table S1. Unit cell parameters (a, c) and its volume (V), the crystallographic and specific densities (ρ), the mass fraction of the hexaferrite phase (ω), the mean particle size (d_m) and standard deviation (σ), the Neel temperatures (T_N), and the Al^{3+} occupancy factors over 2a, 2b, $4f_1$, $4f_2$, 12k iron sites of hexaferrite powder obtained at 1200 °C and ceramic samples $Sr_{1-x/12}Ca_{x/12}Fe_{12-x}Al_xO_{19}$ ($x = 4$) sintered at 1300 and 1400 °C.

Sample	a, Å	c, Å	V, Å^3	ω (HF), %	ρ, g cm^{-3}	ρ^*, %	d_m (σ), μm	T_N, K
powder 1200 °C	5.7856(1)	22.7034(6)	658.13(3)	98.7(2)	4.70(9)	-	0.6 (0.2)	498
ceramics 1300 °C	5.78530(7)	22.7111(3)	658.29(2)	99.5(9)	4.69(4)	70	1.2 (0.4)	498
ceramics 1400 °C	5.7849(1)	22.7238(7)	658.58(3)	100	4.69(8)	99	3.4 (1.1)	507

Sample	2a, %	2b, %	$4f_1$, %	$4f_2$, %	12k, %
powder 1200 °C	75(2)	9(2)	14(1)	13(1)	44
ceramics 1300 °C	75(1)	10(1)	14(1)	13(1)	44
ceramics 1400 °C	76(2)	8(2)	14(1)	12(1)	44

*the specific density was calculated respect to the crystallographic density of 4.70 g cm^{-3} obtained by the Rietveld refinement of the hexaferrite powder sample $Sr_{1-x/12}Ca_{x/12}Fe_{12-x}Al_xO_{19}$ ($x = 4$).
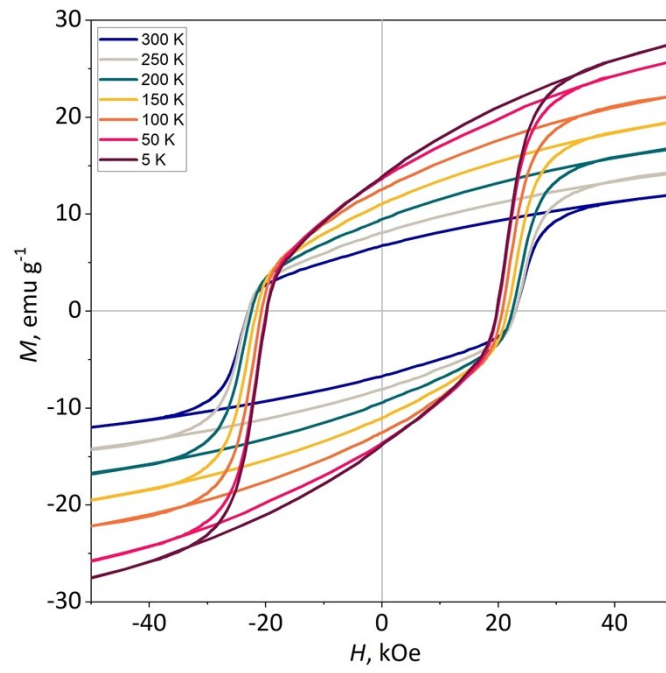
Fig. S3. Temperature dependence of magnetic hysteresis loops of the initial hexaferrite powder of $Sr_{1-x/12}Ca_{x/12}Fe_{12-x}Al_xO_{19}$ (x = 4) annealed at 1200 °C.

Table S2. The coercivity (H_C), the saturation magnetization (M_S), the natural ferromagnetic resonance frequency (f_r), the damping factor or the FWHM (Γ), and Q-factor of the resonance ($Q = f_r \cdot \Gamma^{-1}$) of hexaferrite ceramic samples $Sr_{1-x/12}Ca_{x/12}Fe_{12-x}Al_xO_{19}$ ($x = 4$) sintered at 1300 (left) and 1400 °C (right).

T, K	H_C, kOe	M_S, emu g^{-1}	f_r, GHz	Γ, GHz	Q
300	19.5 | 11.7	13.0 | 11.2	165 | 200	3 | 7	61 | 29
250	19.2 | 11.6	16.2 | 13.4	154 | 198	4 | 5	46 | 40
200	18.8 | 11.5	18.8 | 15.5	158 | 192	3 | 5	48 | 38
150	18.3 | 11.2	21.6 | 17.7	143 | 185	4 | 5	37 | 37
100	17.6 | 10.9	24.2 | 19.7	146 | 178	5 | 5	32 | 36
50	17.2 | −	26.1 | −	140 | 174	3 | 7	47 | 25
5	17.4 | 11.0	26.6 | 21.2	138 | 172	5 | 8	26 | 22

Estimation of Fe^{3+} redistribution

According to the M-type hexaferrite magnetic structure, the following expressions can be written:

$$\frac{[6(1-\alpha_{12k}^{Al^{3+}}) + (1-\alpha_{2a}^{Al^{3+}}) + (1-\alpha_{2b}^{Al^{3+}}) - 2(1-\alpha_{4f_1}^{Al^{3+}}) - 2(1-\alpha_{4f_2}^{Al^{3+}})]}{[6(1-\alpha_{12k}^{Al^{3+}}+x) + (1-\alpha_{2a}^{Al^{3+}}+y) + (1-\alpha_{2b}^{Al^{3+}}+z) - 2(1-\alpha_{4f_1}^{Al^{3+}}+n) - 2(1-\alpha_{4f_2}^{Al^{3+}}+m)]} = \frac{M_S^{1300°C}(T=5K)}{M_S^{1400°C}(T=5K)} = \frac{26.6}{21.2}$$

$$\frac{[6(1-0.44) + (1-0.75) + (1-0.10) - 2(1-0.14) - 2(1-0.13)]}{[6(1-0.44+x) + (1-0.75+y) + (1-0.10+z) - 2(1-0.14+n) - 2(1-0.13+m)]} = \frac{M_S^{1300°C}(T=5K)}{M_S^{1400°C}(T=5K)} = \frac{26.6}{21.2}$$

$$6x + y + z + 2n + 2m = 0$$

Going over the parameters x, y, z, n, m within the range -0.025 … 0.025 with a step 0.001 for the equation and considering the error of the M_S ratio of 3 %, we get about 7,000 relevant sets of parameters, which correspond to the situation when a part of Fe^{3+} moves from spin up (12k, 2a, 2b) to spin down (4f$_1$, 4f$_2$) sites.
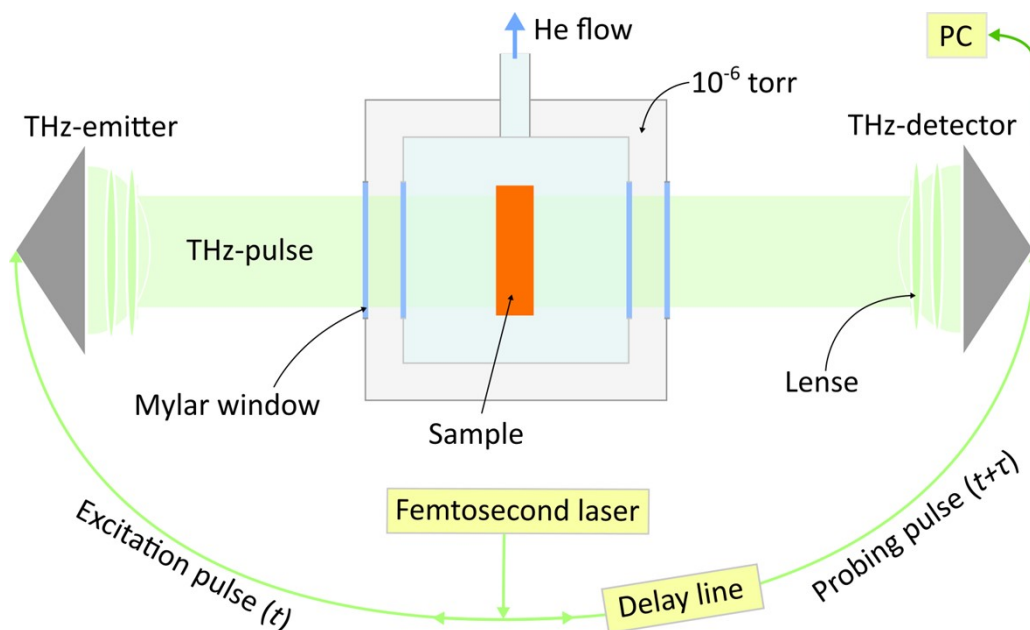
§3. Terahertz spectroscopy

Fig. S4. Zero-field terahertz experiments were performed using the commercial terahertz time-domain spectrometer Menlo Tera K15 [https://www.menlosystems.com/products/thz-time-domain-solutions/terak15-terahertz-spectrometer/]. The standard scheme of the THz-TDS measurements is described in detail [1] and includes a pulse from a femtosecond laser divided into two parts. One part is directed to the photoconductive antenna to perform the THz pulse, and the second is directed to the delay line and further to the detector. The THz pulse probes the sample, and further in the detector body it is scanned by the femtosecond pulse from the delay line. The signal is further elaborated by the computer software. The beam path of the emitted THz pulse includes two TPX and two polyethylene lenses. The sample in the homemade exchange gas cryostat is put in a focus THz beam. The cryostat has a vacuum shield (10^{-6} torr) and an inner sample chamber with the sample holder in the He flow. Temperature is changed by the intensity of He flow and the ceramic heater and is controlled by temperature controllers located in the vicinity of the aperture. Windows in the cryostat are made of mylar, transparent for the THz radiation. The experiment is performed in a sequence of measurements, the first is of the reference signal from the open aperture, and the following is the signal of the radiation passed through the sample with the consequent division of the latter by the former.
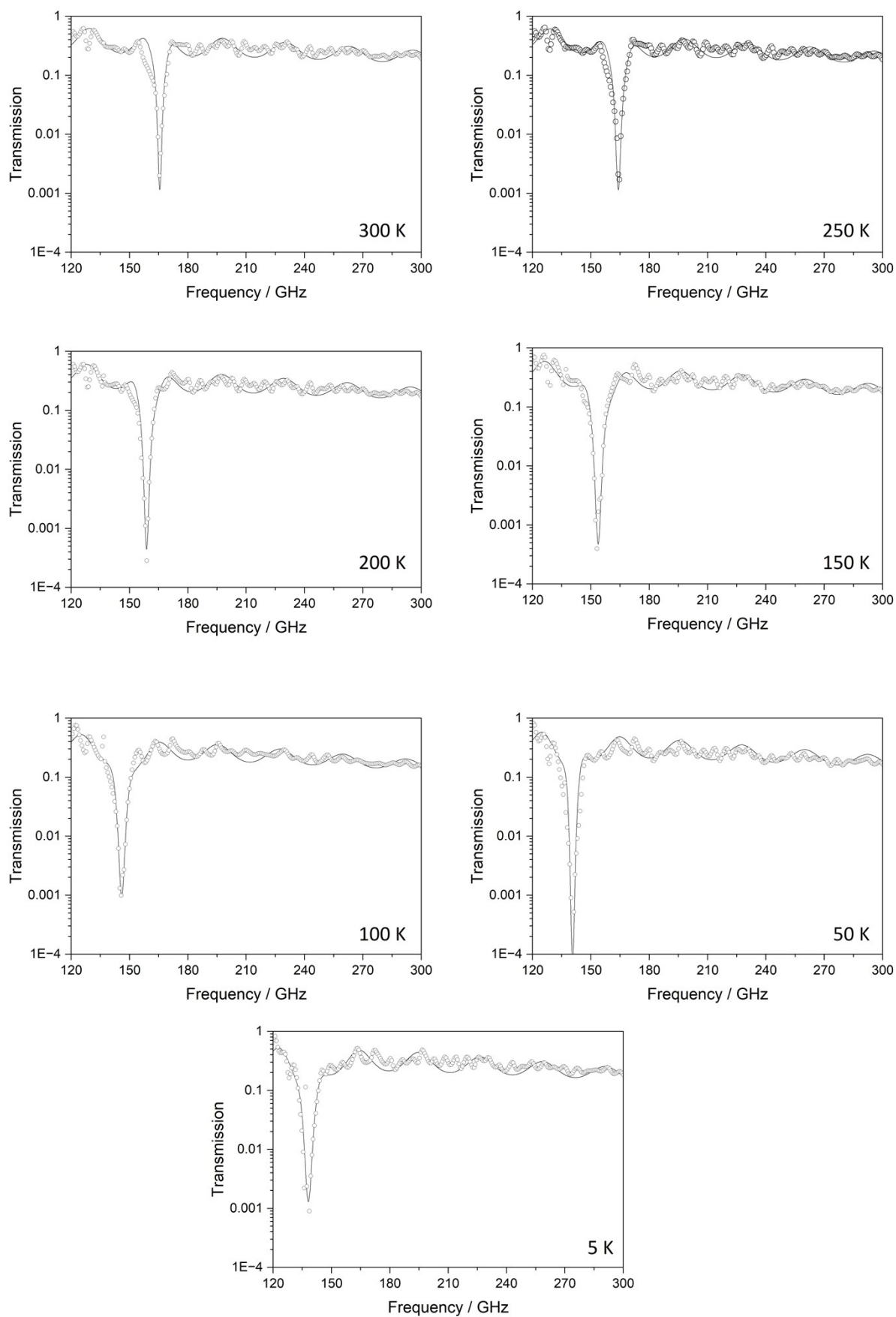
7

Fig. S5. TDS transmission spectra of the ceramics sample $Sr_{1-x/12}Ca_{x/12}Fe_{12-x}Al_xO_{19}$ (x = 4) sintered at 1300 °C (dots) and their fits with a multi-layer model (lines).

Fig. S6. TDS transmission spectra of the ceramics sample $Sr_{1-x/12}Ca_{x/12}Fe_{12-x}Al_xO_{19}$ ($x = 4$) sintered at 1400 °C (dots) and their fits with a multi-layer model (lines).
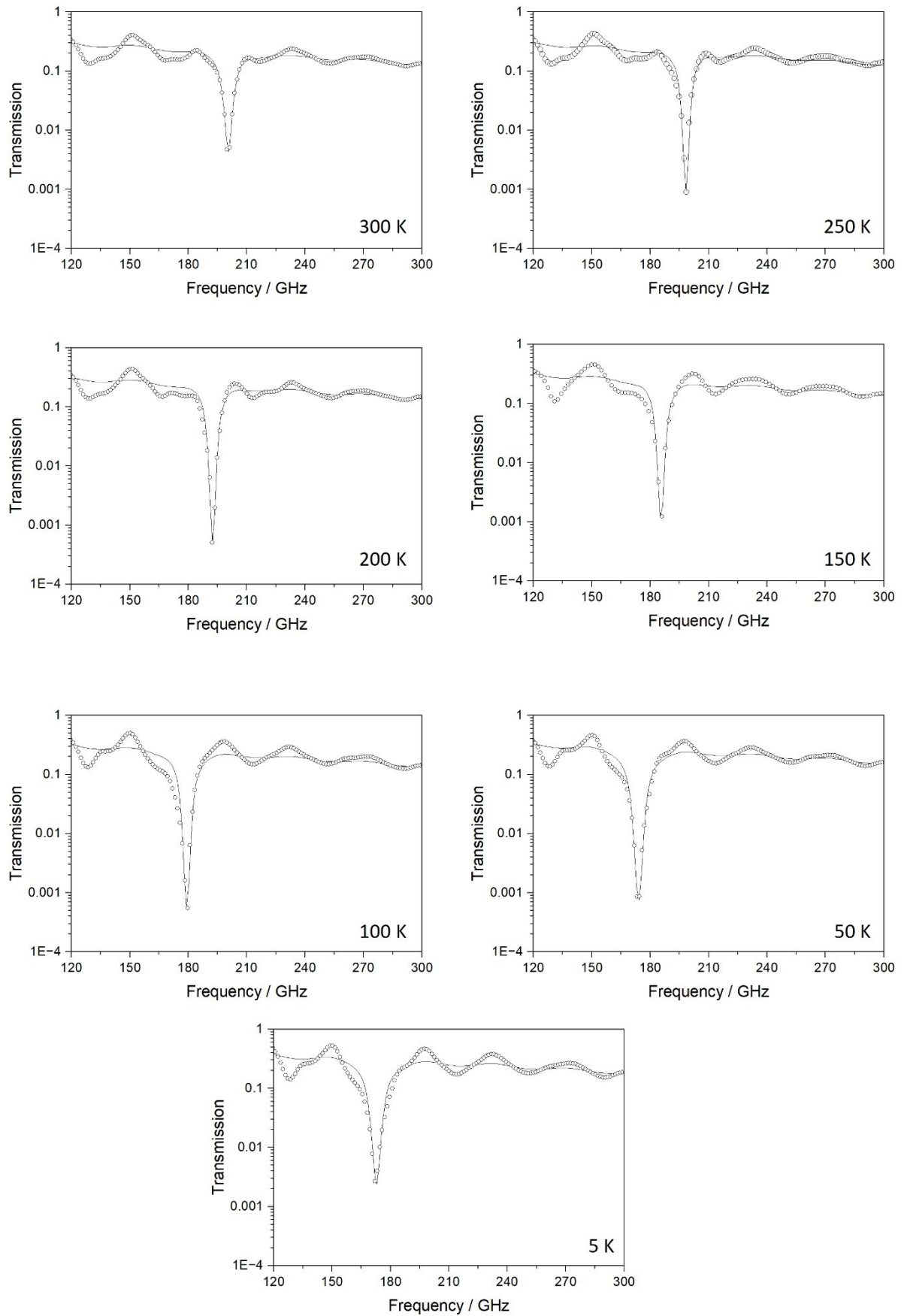
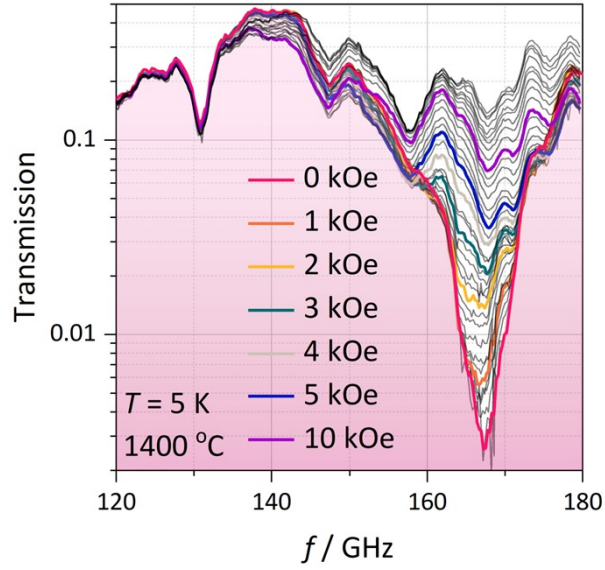**Fig. S7**. Ferromagnetic resonance spectra of initially non-magnetized hexaferrite ceramics ($Sr_{1-x/12}Ca_{x/12}Fe_{12-x}Al_xO_{19}$, $x = 4$, sintered at 1400 °C) measured at 5 K under an external magnetic field (0… +50 kOe).

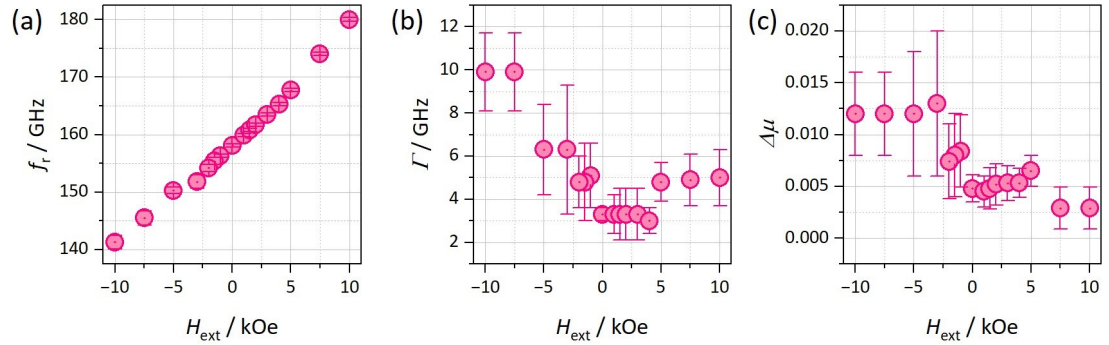**Fig. S8**. Ferromagnetic resonance spectra of the magnetized (remanent) hexaferrite ceramics ($Sr_{1-x/12}Ca_{x/12}Fe_{12-x}Al_xO_{19}$, $x = 4$, sintered at 1300 °C) measured at 130 K under external magnetic field (-10… +10 kOe).

To determine the parameters of resonance absorption, a multi-layer model for transmission coefficient was used to account for standing waves in the optical path inside the cryostat that appear due to multiple reflections (Fabry-Perot effect) of the radiation between outer and inner Mylar windows of the cryostat, between inner windows and sample surface and between sample faces (within the sample), see Fig. 2a and Fig. S4. Such an approach allowed to account for additional wavy structure in the spectra of transmission coefficient (see, e.g., Figures 3a,b,c and Figures S5, S6 and S7), and thus to reliably determine the resonance parameters. The analysis was performed with the WASF software with built-in standard Fresnel expressions for optical properties (transmission, reflection, absorption) of multi-layer systems, of the type B26-B29 presented in [Dressel, M.; Gruner, G. Electrodynamics of Solids Cambridge University Press. Cambridge, UK 2002].

§3. Modeling and calculations

Micromagnetic modeling

The energy equations which were combined to minimize the total energy of the system:

1) Zeeman energy: $-\mu_0 M_S m \cdot H_{ext}$;
2) Uniaxial anisotropy energy: $-K(m \cdot u)^2$;
3) Exchange energy: $-Am \cdot \nabla^2 m$;
4) Magnetostatic energy: $-\frac{1}{2}\mu_0 M_S m \cdot H_d$,

where M_S – the saturation magnetization; **m** – unit vector of the magnetization; **H_ext** – vector of an external magnetic field; K – magnetocrystalline anisotropy constant; **u** – unit vector of the anisotropy field (H_a); **A** – exchange energy constant; **H_d** – vector of a demagnetization field, the calculation procedure of which can be found in [2].

The value of the M_S was calculated as follows:

M_S = (1000/4π) · 4π ·ρ·M_{90} = 1000 · 4.69 g cm^{-3} · 22.5 emu g^{-1} ≈ 106 kA m^{-1}, where ρ – crystallographic density calculated by the Rietveld refinement method, M_{90} – an experimental value of the saturation magnetization, which was refined by a linear interpolation according to the corresponding temperature of the FMR measurements.

The value of the K_1 was calculated using Kittel's formular [3] as follows:

f_r = (γ/2π)·2K_1/(ρ·M_{90}), then K_1 = π · f_r · ρ·M_{90}/γ, where f_r – an experimental value of the ferromagnetic resonance frequency at zero magnetic field, γ/2π = 2.8 GHz/kOe (value of the gyromagnetic ratio for the M-type hexaferrites, as g-factor ≈ 2) [4]. As obtained [K_1] = Merg cm^{-3} was converted into kJ m^{-3} by a multiplication factor of 100.

Figure S9 illustrates ferromagnetic resonance precession with labels of vectors, which are used in the Landau-Lifshits equation to calculate the magnetic susceptibility spectra $\chi(f)$ and in the equations of the "Spin current" section to calculate the DC spin currents.
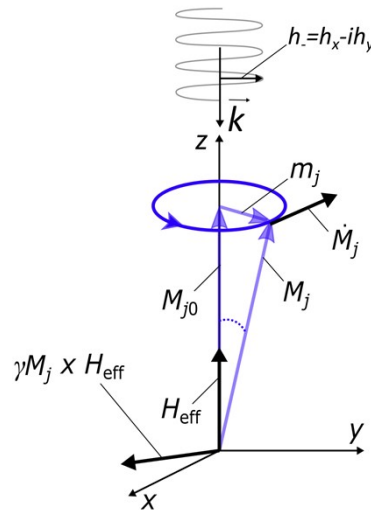

Fig. S9. Precession of magnetization in a ferromagnet and a falling circular polarized EM wave with an oscillating vector *h*, which can be absorbed by the right-handed precession (FMR mode).

To calculate $\chi(f)$ spectra, we used the Landau-Lifshits equation for a ferromagnet (with only magnetic sublattice j):

$$\dot{M}_j = -\gamma M_j \times H_{eff,j} + \frac{\alpha}{M_{j0}} M_j \times \dot{M}_j ,$$

where H_{eff} – an effective magnetic field, i.e., superposition of an external magnetic field (H_{ext}), anisotropy field (H_a), an exchange field (H_{ex}), a demagnetization field (H_d), and AC magnetic field of EM wave (he^{ift}). M_{0j} was considered as M_S.

Spin current

By definition, the spin current can be expressed as [5]:

$$J_s = (\hbar/4\pi) g_r^{\uparrow\downarrow} M \times M ,$$

where $g_r^{\uparrow\downarrow}$ denotes the spin-mixing conductance.

To write this expression in a more physical form, we calculate $M \times M$ by parameterizing as:

$$M = \begin{cases} m_j cos(ft) \\ \pm m_j sin(ft) \\ M_{j0} \end{cases}$$

Considering a precession of the magnetic moment around the z-axis, it can be concluded that the currents flowing in the plane, which is basal to the axis, will compensate each other when averaging over time. Thus, to fully judge the spin current, it is enough to consider only its z-component. By solving the Landau-Lifshitz equations for the corresponding magnetic systems, we obtained the z-projection of the DC spin current:

$$J_{s,z}^{DC} = (\hbar/4\pi) g_r^{\uparrow\downarrow} f_r m_{\pm}^2 = (\hbar/4\pi) g_r^{\uparrow\downarrow} f_r \chi_r^{"2} h^2$$

Also, solving Landau-Lifshitz for the simplest case (for two-magnetic-sublattice ferrimagnetic) for the condition the anisotropy field is much lower than the molecular field (exchange field) $H_a \ll H_{ex}$, we get the expression for the imaginary part of the magnetic susceptibility:

$$\chi_r^{"} = \frac{\gamma M_S}{\alpha f_r} = \frac{\gamma M_S}{\Gamma}$$

To calculate the DC spin current J_z^{DC} in units of $(\hbar/4\pi) g_r^{\uparrow\downarrow} h^2$ for the hexaferrite and epsilon iron oxide samples, we have taken the measured NFMR frequency, experimental damping factor Γ, the saturation magnetization at 90 kOe multiplied by the crystallographic density of the compound (obtained from the Rietveld refinement in case of the hexaferrites, and 4.73 g cm^{-3} for ε-Fe$_2$O$_3$), γ = 2.8 GHz kOe^{-1}. The data for the epsilon iron oxide was taken from our previous work [6].

In the same way, for the antiferromagnetic resonance, the following expressions are valid:

$$f_{AFMR\pm} = \gamma[\sqrt{(2H_E + H_a)H_a} \pm H_{ext}],$$

where H_{ext} is an external magnetic field.

$$\chi_r^{"} = \frac{\gamma M_0 H_a}{\alpha(H_{ex} + H_a) f_r}$$

To model J_z^{DC} for the antiferromagnetic resonance in MnF$_2$, we have taken the following parameters: H_a = 8800 Oe, H_{ex} = 556 000 Oe, M_0 = 590 G at 0 K, and the highest f_r = 261 GHz at 4.2 K from [7]; and γ = 0.0028 GHz Oe^{-1}, α = 0.01 (Γ = 2.61 GHz). Thus, the $J_z^{DC} \approx 0.025$ units of $(\hbar/4\pi) g_r^{\uparrow\downarrow} h^2$.

References

1   M. C. Nuss and J. Orenstein, in *Millimeter and Submillimeter Wave Spectroscopy of Solids*, Springer Berlin Heidelberg, 1998, pp. 7–50.
2   C. Abert, F. Bruckner, C. Vogler, R. Windl, R. Thanhoffer and D. Suess, *J. Magn. Magn. Mater.*, 2015, **387**, 13–18.
3   C. Kittel, *Phys. Rev.*, 1948, **73**, 155–161.
4   A. B. Ustinov, A. S. Tatarenko, G. Srinivasan and A. M. Balbashov, *J. Appl. Phys.*, 2009, **105**, 023908.
5   V. Baltz, A. Manchon, M. Tsoi, T. Moriyama, T. Ono and Y. Tserkovnyak, *Rev. Mod. Phys.*, 2018, **90**, 015005.
6   E. A. Gorbachev, L. N. Alyabyeva, M. V. Soshnikov, V. A. Lebedev, A. V. Morozov, E. S. Kozlyakova, A. Ahmed, A. A. Eliseev and L. A. Trusov, *Mater. Horizons*, 2023, **10**, 3631–3642.
7   F. M. Johnson and A. H. Nethercot, *Phys. Rev.*, 1959, **114**, 705–716.